Interdependence of Electronic and Thermal Transport in $Al_xGa_{1-x}N$ Channel HEMTs

Bikramjit Chatterjee, James Spencer Lundh, Yiwen Song, Daniel Shoemaker, Albert G. Baca, Robert J. Kaplar, Thomas E. Beechem, Christopher Saltonstall, Andrew A. Allerman, Andrew M. Armstrong, Brianna A. Klein, Anushka Bansal, Hamid R. Seyf, Disha Talreja, Alexej Pogrebnyakov, Eric Heller, Venkatraman Gopalan, Asegun S. Henry, Joan M. Redwing, Brian Foley, and Sukwon Choi

***Abstract*— Aluminum gallium nitride (AlGaN) high electron mobility transistors (HEMTs) are candidates for next-generation power conversion and radio frequency (RF) applications. Al_xGa_{1-x} N channel HEMT devices (x = 0.3, x = 0.7) were investigated using multiple in-situ thermal characterization methods and electro-thermal simulation. The thermal conductivity, contact resistivity, and channel mobility were characterized as a function of temperature to understand and compare the heat generation profile and electro-thermal transport within these devices. In contrast to GaN-based HEMTs, the electrical output characteristics of $Al_{0.70}Ga_{0.30}$ N channel HEMTs exhibit remarkably lower sensitivity to the ambient temperature rise. Also, during 10kHz pulsed operation, the difference in peak temperature between the AlGaN channel HEMTs and GaN HEMTs reduced significantly.**

***Index Terms*— AlGaN HEMT, Raman thermography, thermoreflectance imaging, electro-thermal characterization.**

Manuscript received January 9, 2020; accepted January 21, 2020. Date of publication January 27, 2020; date of current version February 25, 2020. This work was supported in part by the AFOSR Young Investigator Program under Grant FA9550-17-1-0141, in part by the NSF under Grant DMR-1808900, and in part by the Penn State NSF-MRSEC Center for Nanoscale Science under Grant DMR 1420620. Sandia National Laboratories is a multi-mission laboratory managed and operated by National Technology and Engineering Solutions of Sandia, LLC, a wholly owned subsidiary of Honeywell International Inc., for the U.S. Department of Energy's National Nuclear Security Administration, under Grant DE-NA0003525. The review of this letter was arranged by Editor D. G. Senesky. *(Corresponding author: Sukwon Choi.)*

Bikramjit Chatterjee, James Spencer Lundh, Yiwen Song, Daniel Shoemaker, Brian Foley, and Sukwon Choi are with the Department of Mechanical Engineering, The Pennsylvania State University, University Park, PA 16802 USA (e-mail: sukwon.choi@psu.edu).

Albert G. Baca, Robert J. Kaplar, Thomas E. Beechem, Christopher Saltonstall, Andrew A. Allerman, Andrew M. Armstrong, and Brianna A. Klein are with Sandia National Laboratories, Albuquerque, NM 87185 USA.

Anushka Bansal, Disha Talreja, Alexej Pogrebnyakov, Venkatraman Gopalan, and Joan M. Redwing are with the Department of Materials Science and Engineering, The Pennsylvania State University, University Park, PA 16802 USA.

Hamid R. Seyf is with the School of Mechanical Engineering, Purdue University, West Lafayette, IN 47907 USA.

Eric Heller is with the Materials and Manufacturing Directorate, Air Force Research Laboratory, Wright-Patterson Air Force Base, OH 45433 USA.

Asegun S. Henry is with the Department of Mechanical Engineering, Massachusetts Institute of Technology, Cambridge, MA 02139 USA.

Color versions of one or more of the figures in this letter are available online at http://ieeexplore.ieee.org.

Digital Object Identifier 10.1109/LED.2020.2969515

I. Introduction

ULTRA-WIDE bandgap devices based on AlGaN, β-Ga_2O_3, and diamond give promise to surpass GaN lateral transistors for radio frequency (RF) and power switching applications [1]. Among these materials, AlGaN uniquely possesses spontaneous and piezoelectric polarization enabling HEMTs similar to today's GaN-based HEMTs but with higher breakdown voltage (due to the wider bandgap) and lower intrinsic carrier concentration at high temperatures [2]–[4]. Moreover, the AlGaN system can readily take advantage of the manufacturing infrastructure for GaN-based commercial electronic and optoelectronic devices.

While higher Al mole fraction x is favored from a breakdown voltage standpoint, the fabrication of ohmic contact resistance becomes challenging for wider bandgap materials [3], [5]. Moreover, alloying causes the thermal conductivity (κ) and channel mobility (μ) to significantly reduce as compared to those for the binary constituents GaN and AlN [5]. However, the disadvantage due to smaller low-field μ can be alleviated by scaling the devices for RF applications such that the electronic transport is governed by the saturation velocity (v_{sat} $\sim 2\times10^7$ cm/s) rather than μ [1]. Moreover, as the low-field μ of the two dimensional electron gas (2DEG) formed in AlGaN is governed by alloy scattering, the rate of mobility degradation with temperature for AlGaN is smaller than that of GaN [1], [3]. This offers a potential benefit to employ AlGaN instead of GaN in RF applications where the environment temperature exceeds 200°C [1]. It is crucial to understand the implicit interdependence of these variables that govern the electronic and thermal transport, as any variation in μ and specific contact resistivity (ρ_c) have direct impact on the device heat generation distribution, whereas κ determines the channel temperature rise, influencing μ and ρ_c. In response to this, temperature dependent κ and ρ_c measurements were carried out for AlGaN-channel HEMTs with varying Al mole fraction (the temperature and compositional dependences of μ have been reported in our previous work [3]). The cumulative effect of these variables on the heat generation and channel temperature distributions of AlGaN transmission line measurement (TLM) structures and HEMTs was investigated using electro-thermal simulation [6], [7] and optical thermography techniques [8]–[10].

II. Device Description

$Al_xGa_{1-x}N$ channel HEMTs (x = 0.3 and x = 0.7) were grown via metal organic chemical vapor deposition (MOCVD) on sapphire substrates. The Al mole fraction for the

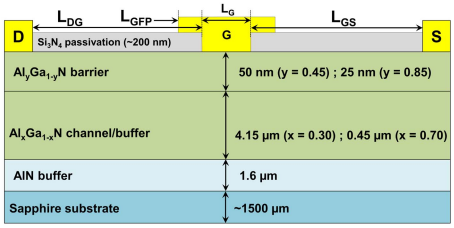

Fig. 1. Schematic cross-section of the device types that were studied.

$Al_yGa_{1-y}N$ barriers were y = 0.45 and y = 0.85, respectively (Fig. 1) [4], [11]. Henceforth, these devices will be referred to as 45/30 and 85/70 HEMTs, respectively. To further investigate the impact of ohmic contact resistance on the device electro-thermal performance, the 85/70 HEMTs were designed with two different levels of source/drain contact resistance (henceforth referred to as high-R_c and low-R_c HEMTs). The 45/30 and high-R_c 85/70 devices employed planar Ti/Al/Ni/Au ohmic contacts while the low-R_c 85/70 devices adopted planar Zr/Al/Mo/Au ohmic contacts [12]. TLM structures with identical material stack layouts were also fabricated.

III. Variables Governing Electro-Thermal Transport

The κ of MOCVD-grown $Al_xGa_{1-x}N$ layers for varying x were measured via time and frequency domain thermoreflectance methods [13], [14] and numerically calculated using the virtual crystal approximation (VCA) model [15], [16]. 85 nm Au/Ti metal transducers were deposited on $Al_xGa_{1-x}N$ (1 μm)/AlN (90 nm)/6H-SiC (0001) samples for the measurements. κ was found to drop sharply as the composition of AlGaN approaches ~10% (x = 0.1) and then it remains approximately constant until ~90% after which it quickly increases to the AlN κ (Fig. 2(a)). The sharp drop of κ vs. x is due to strong scattering mechanisms arising from alloying and is consistent with other measurements of κ in alloys [15], [16]. κ values for single crystal thin film GaN (130 W/mK) and AlN (240 W/mK) are also shown in Fig. 2(a) [13], [17].

The κ of 30% and 70% Al fraction $Al_xGa_{1-x}N$ were measured for a wide range of temperatures (Fig. 2(b)). At room temperature, the κ of $Al_{0.3}Ga_{0.7}N$ and $Al_{0.7}Ga_{0.3}N$ were 8.8 ± 0.54 W/mK and 9.7 ± 0.29 W/mK, respectively (added to Fig. 2(a) for comparison with results obtained from TDTR). Interestingly, a negligible reduction in κ with increasing temperature is observed for both compositions in contrast to the κ of GaN and AlN [18]–[20], both of which monotonically decrease with temperature. The random substitution of Al (Ga) atoms within the group-III cationic sublattice complicates the vibrational mode character of the ternary alloy system. Accordingly, correlated interactions between phonon-like propagating vibrational modes and non-propagating modes such as diffusions [16] result in the weak temperature dependence of the AlGaN κ.

Contact resistances for all devices were measured using TLM structures. At room temperature, the measured ρ_c for the 45/30 TLMs, low-R_c 85/70 TLMs, and high-R_c 85/70 TLMs were $5.83\times10^{-5}\Omega$-cm^2, $8.88\times10^{-4}\Omega$-cm^2, and $1.76\times10^{-3}\Omega$-cm^2, respectively. However, these resistivities will change due to device self-heating during operation as ρ_c is a strong function of temperature, as shown in Fig. 2(c). The reduction of $\rho_c$with increasing temperature (ΔT) is indicative of thermionic emission contributions to conduction [12]. Change of mobility for the 45/30 and 85/70 HEMTs were derived from the same measurements (ignoring the change in 2DEG density with temperature rise as shown in [3], [21], [22]) and shown in the right-Y axis of Fig. 2(c). The results show that the rate of reduction in μ for the 85/70 HEMTs is 44% lower than that of the 45/30 HEMTs for the temperature range of 25°C to 125°C. The results agree with our previous work [3]. All of these trends will affect the electro-thermal transport of the HEMTs.

IV. Heat Generation and Self-Heating

Fig. 3(a) and (b) show the measured output and transfer characteristics of the 45/30 and 85/70 HEMTs. To understand electro-thermal self-heating mechanisms, 3D electro-thermal models of the tested structures that couple a 2D electrical model (Synopsys Sentaurus) with a 3D finite element thermal model (COMSOL Multiphysics) [23] were constructed. Electronic and material properties including bandgap energy and dielectric constant were adopted from values reported in literature [3], [24]. Measured values of κ, ρ_c, and μ of the $Al_xGa_{1-x}N$ materials were used. As can be seen in Fig. 3(a), the simulated electrical output characteristics show excellent agreement with measured data. Similar validated models for TLM structures were used to study the effect of contact resistance on the distribution of heat generation (q''') along the channel. Due to the >10× higher contact resistance for the 85/70 TLMs, a much larger fraction (93% for low-R_cTLMs and 97% for high-R_c TLMs) of the total input power ($P = I\cdot V$) is dissipated at the drain and source contacts as compared to the 45/30 TLMs (9%) (Fig. 3(c)). This in turn leads to a significantly different trend in the temperature distributions when comparing the 45/30 and 85/70 TLMs as is observed by thermoreflectance and Raman thermography [25] results shown in Fig. 3 (d). The 45/30 TLMs exhibit a channel temperature rise which is 82% higher than their contact temperature at a power density of 1.59 W/mm. In contrast, for the same power density, both low R_c and high R_c 85/70 TLMs show comparable channel and contact temperatures.

Fig. 3 (e) shows the q''' distributions across the channels of the 45/30 HEMT and low-R_c 85/70 HEMT for P = 500 mW under identical pinched-off channel conditions (V_{GS} values were adjusted such that I_D values were 50% of those for fully-open channel conditions) to preclude bias-dependent variation of the heat generation profile due to field effects [6], [26]. To account for differences in the channel width (W_{ch}) and power dissipation in the channel (Q_{ch}) for the two HEMTs, q''' has been normalized. Due to the higher ρ_c in the 85/70 HEMT, the total q''' in the channel is much lower than that for the 45/30 HEMT (Fig. 3(e), top). The higher peak amplitude of q''' (Fig. 3(e), bottom) for the 85/70 HEMT causes a sharper temperature gradient in the ΔT distribution as shown in Fig. 3(f). However, the slightly lower thermal conductivity of $Al_{0.3}Ga_{0.7}N$ and different AlGaN channel/buffer layer thicknesses are factors leading to higher peak ΔT for the 45/30 HEMT.

V. Device Performance

The low κ (and thus, low thermal diffusivity, α) of AlGaN results in large thermal time constants for the AlGaN devices [10]. Consequently, under moderately high frequency switching conditions (10 kHz), the ΔT of the AlGaN channel HEMTs is <60% (53% for 45/30 and 41% for low-R_c 85/70) of the steady-state temperature rise under direct current (DC) operation. Hence, the intense self-heating effect in AlGaN HEMTs is mitigated under high-frequency pulse-mode operations as employed in industry motors

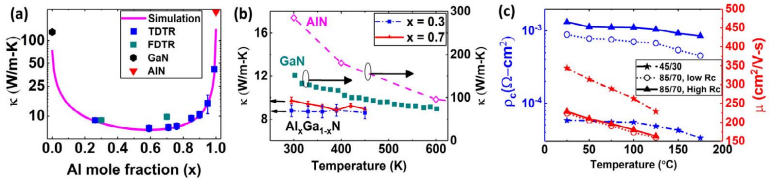

Fig. 2. (a) Mole fraction dependent thermal conductivity of $Al_xGa_{1-x}N$ thin films at 25°C. (b) The temperature dependent thermal conductivities of $Al_xGa_{1-x}N$ for x = 0.3 and x = 0.7 for a temperature range of 300 − 450 K. κ(T) for bulk AlN and a GaN film are also plotted. (c) Temperature dependence of ρc and μ fo r the TLMs.

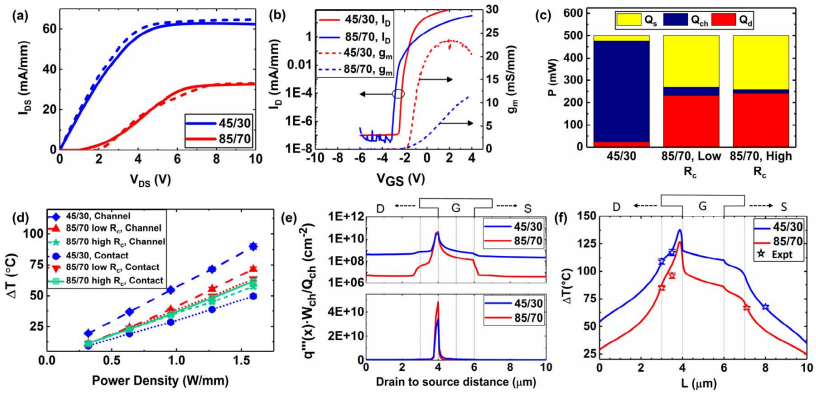

Fig. 3. (a) Measured and simulated output characteristics for the 45/30 and 85/70 (low R_c) HEMTs. (b) Measured I_D and transconductance (g_m) for the 45/30 and 85/70 (low R_c) HEMTs. (c) Heat generation in the ohmic contacts (Q_s, Q_d) and AlGaN channel (Q_{ch}) for 45/30, low R_c 85/70, and high R_c 85/70 TLMs. (d) Temperature rise in the 45/30, low R_c 85/70, and high R_c 85/70 TLMs due to self-heating. (e) Channel heat generation distribution for the 45/30 and low R_c 85/70 HEMTs at the same power dissipation (500 mW) on log (top) and linear (bottom) scales. Channel is 50% open for both cases. (f) Temperature rise across the channel for the 45/30 and low R_c 85/70 HEMTs. Experimental data includes thermoreflectance imaging and Raman thermography results.

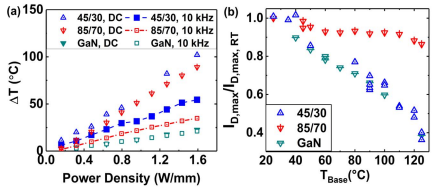

Fig. 4. (a) Temperature rise for the HEMTs under DC and 10 kHz pulsed conditions. (b) Reduction in $I_{D,max}$ for varying thermal stage temperature.

and AC-DC/DC-DC converters [27], [28]. A standard GaN channel HEMT (structural details in Reference [7]) was characterized for comparison with the AlGaN HEMTs. Due to the higher κ of the GaN material, the measured steady-state and 10 kHz pulsed (10% duty cycle) channel temperatures are nearly identical (ΔT_{Pulse} ~95% of ΔT_{DC} at 1.59 W/mm power density, Fig. 4(a)).

Fig. 4(b) shows that $I_{D,max}$ (the drain current at the "knee" of the output characteristic curves) of the 85/70 HEMT at ΔT of 100°C reduces by 14% as compared to its room-temperature value. In contrast, a ~60% reduction is observed for both the 45/30 and the GaN HEMTs. This weak temperature dependence is partly attributed to the relatively temperature insensitive mobility for higher Al mole fraction $Al_xGa_{1-x}N$ and partly due to the fact that contact resistance improves with temperature, as shown in Fig. 2 (c) [3], [12]. Quantitatively, the increase in R_{sh} due to temperature increase from 25°C to 125°C can be measured to be 80% larger for the 45/30 HEMTs (2180Ω/□) as compared to the 85/70 HEMTs (1210Ω/□). To further compare the fractional contribution of decrease in contact resistance and increase in sheet resistance with temperature, a factor φ can be defined as follows.

$$\varphi = \left[R_c(25°C) - R_c(125°C)\right] / \left[R_{sh}(125°C) - R_{sh}(25°C)\right] \quad (1)$$

Using the data shown in Fig. 2 (c), the value of φ was found to be 82% higher for the 85/70 HEMTs (0.33) than the 45/30 HEMT (0.18). This implies the contribution of reduction in contact resistance towards the increase in total resistance due to temperature rise is significantly higher (2.2×) for the 85/70 HEMTs. However, the relatively less degradation of mobility in the 85/70 HEMTs result in 32% smaller temperature-induced reduction in sheet resistance. Hence, the net effect of both of these factors results in a relatively temperature-insensitive $I_{D,max}$ for the 85/70 HEMT which is favorable for their potential use in extreme temperature applications (e.g., down-hole exploration, aircraft/rocket engine control, and space exploration) that require stable operation at high ambient temperature conditions, comparable to the room temperature performance [21].

VI. Conclusion

The high ρ_c of 85/70 HEMTs resulted in markedly different heat generation and temperature distributions as compared to 45/30 HEMTs. Although the ΔT of the 85/70 AlGaN HEMTs was four times that of GaN channel HEMTs, the temperature insensitive μ and κ, along with the improvement in ρ_c, were shown to lead to stable electrical output characteristics at high ambient temperature conditions. The low κ (and hence, low α) of the AlGaN also contributes to a lower ΔT under pulsed operating conditions as compared to ΔT under DC operation, thus reducing self-heating concerns. For reliability-critical applications, thermal management solutions such as flip-chip hetero-integration [29] and substrate integration methods [30] can be implemented to further mitigate self-heating effects.

Acknowledgment

This paper describes objective technical results and analysis. Any subjective views or opinions that might be expressed in the paper do not necessarily represent the views of the U.S. Department of Energy or the United States Government.

REFERENCES

[1] S. Reza, B. A. Klein, A. G. Baca, A. M. Armstrong, A. A. Allerman, E. A. Douglas, and R. J. Kaplar, "High-frequency, high-power performance of AlGaN-channel high-electron-mobility transistors: An RF simulation study," *Jpn. J. Appl. Phys.*, vol. 58, Jun. 2019, Art. no. SCCD04, doi: 10.7567/1347-4065/ab07a5.

[2] O. Ambacher, J. Smart, J. R. Shealy, N. G. Weimann, K. Chu, M. Murphy, W. J. Schaff, L. F. Eastman, R. Dimitrov, L. Wittmer, M. Stutzmann, W. Rieger, and J. Hilsenbeck, "Two-dimensional electron gases induced by spontaneous and piezoelectric polarization charges in N- and Ga-face AlGaN/GaN heterostructures," *J. Appl. Phys.*, vol. 85, no. 6, pp. 3222–3233, Mar. 1999, doi: 10.1063/1.369664.

[3] M. E. Coltrin, A. G. Baca, and R. J. Kaplar, "Analysis of 2D transport and performance characteristics for lateral power devices based on AlGaN alloys," *ECS J. Solid State Sci. Technol.*, vol. 6, no. 11, pp. S3114–S3118, 2017, doi: 10.1149/2.0241711jss.

[4] A. G. Baca, B. A. Klein, A. A. Allerman, A. M. Armstrong, E. A. Douglas, C. A. Stephenson, T. R. Fortune, and R. J. Kaplar, "$Al_{0.85}Ga_{0.15}N/Al_{0.70}Ga_{0.30}N$ high electron mobility transistors with Schottky gates and large on/off current ratio over temperature," *ECS J. Solid State Sci. Technol.*, vol. 6, no. 12, pp. Q161–Q165, 2017, doi: 10.1149/2.0231712jss.

[5] W. Liu and A. A. Balandin, "Thermal conduction in $Al_xGa_{1-x}N$ alloys and thin films," *J. Appl. Phys.*, vol. 97, no. 7, 2005, Art. no. 073710, doi: 10.1063/1.1868876.

[6] E. R. Heller and A. Crespo, "Electro-thermal modeling of multi-finger AlGaN/GaN HEMT device operation including thermal substrate effects," *Microelectron. Rel.*, vol. 48, no. 1, pp. 45–50, 2008, doi: 10.1016/j.microrel.2007.01.090.

[7] B. Chatterjee, J. S. Lundh, J. Dallas, H. Kim, and S. Choi, "Electro-thermal reliability study of GaN high electron mobility transistors," in *Proc. 16th IEEE Intersoc. Conf. Therm. Thermomech.Phenomena Electron. Syst. (ITherm)*, May 2017, pp. 1247–1252, doi: 10.1109/itherm.2017.7992627.

[8] K. Maize, E. Heller, D. Dorsey, and A. Shakouri, "Thermoreflectance CCD imaging of self heating in AlGaN/GaN high electron mobility power transistors at high drain voltage," in *Proc. 28th Annu. IEEE Semiconductor Therm. Meas. Manage. Symp. (SEMI-THERM)*, Mar. 2012, pp. 173–181, doi: 10.1109/stherm.2012.6188846.

[9] B. Chatterjee, A. Jayawardena, E. Heller, D. W. Snyder, S. Dhar, and S. Choi, "Thermal characterization of gallium oxide Schottky barrier diodes," *Rev. Sci. Instrum.*, vol. 89, no. 11, Nov. 2018, Art. no. 114903, doi: 10.1063/1.5053621.

[10] B. Chatterjee, K. Zeng, C. D. Nordquist, U. Singisetti, and S. Choi, "Device-level thermal management of gallium oxide field-effect transistors," *IEEE Trans. Compon., Packag., Manuf. Technol.*, vol. 9, no. 12, pp. 2352–2365, Dec. 2019, doi: 10.1109/tcpmt.2019.2923356.

[11] A. G. Baca, A. M. Armstrong, A. A. Allerman, B. A. Klein, E. A. Douglas, C. A. Sanchez, and T. R. Fortune, "High temperature operation of $Al_{0.45}Ga_{0.55}N/Al_{0.30}Ga_{0.70}N$ high electron mobility transistors," *ECS J. Solid State Sci. Technol.*, vol. 6, no. 11, pp. S3010–S3013, 2017, doi: 10.1149/2.0041711jss.

[12] B. A. Klein, A. G. Baca, A. M. Armstrong, A. A. Allerman, C. A. Sanchez, E. A. Douglas, M. H. Crawford, M. A. Miller, P. G. Kotula, T. R. Fortune, and V. M. Abate, "Planar ohmic contacts to $Al_{0.45}Ga_{0.55}N/Al_{0.3}Ga_{0.7}N$ high electron mobility transistors," *ECS J. Solid State Sci. Technol.*, vol. 6, no. 11, pp. S3067–S3071, 2017, doi: 10.1149/2.0181711jss.

[13] T. E. Beechem, A. E. Mcdonald, E. J. Fuller, A. A. Talin, C. M. Rost, J.-P. Maria, J. T. Gaskins, P. E. Hopkins, and A. A. Allerman, "Size dictated thermal conductivity of GaN," *J. Appl. Phys.*, vol. 120, no. 9, Sep. 2016, Art. no. 095104, doi: 10.1063/1.4962010.

[14] J. Yang, C. Maragliano, and A. J. Schmidt, "Thermal property microscopy with frequency domain thermoreflectance," *Rev. Sci. Instrum.*, vol. 84, no. 10, Oct. 2013, Art. no. 104904, doi: 10.1063/1.4824143.

[15] Z. Wang and N. Mingo, "Diameter dependence of SiGe nanowire thermal conductivity," *Appl. Phys. Lett.*, vol. 97, no. 10, Sep. 2010, Art. no. 101903, doi: 10.1063/1.3486171.

[16] H. R. Seyf, L. Yates, T. L. Bougher, S. Graham, B. A. Cola, T. Detchprohm, M.-H. Ji, J. Kim, R. Dupuis, W. Lv, and A. Henry, "Rethinking phonons: The issue of disorder," *npj Comput. Mater.*, vol. 3, no. 1, p. 49, 2017, doi: 10.1038/s41524-017-0052-9.

[17] R. L. Xu, M. M. Rojo, S. M. Islam, A. Sood, B. Vareskic, A. Katre, N. Mingo, K. E. Goodson, H. G. Xing, D. Jena, and E. Pop, "Thermal conductivity of crystalline AlN and the influence of atomic-scale defects," *J. Appl. Phys.*, vol. 126, no. 18, Nov. 2019, Art. no. 185105, doi: 10.1063/1.5097172.

[18] H. Guo, Y. Kong, and T. Chen, "Thermal simulation of high power GaN-on-diamond substrates for HEMT applications," *Diamond Rel. Mater.*, vol. 73, pp. 260–266, Mar. 2017, doi: 10.1016/j.diamond.2016.10.006.

[19] J. Das, H. Oprins, H. Ji, A. Sarua, W. Ruythooren, J. Derluyn, M. Kuball, M. Germain, and G. Borghs, "Improved thermal performance of AlGaN/GaN HEMTs by an optimized flip-chip design," *IEEE Trans. Electron Devices*, vol. 53, no. 11, pp. 2696–2702, Nov. 2006, doi: 10.1109/TED.2006.883944.

[20] G. A. Slack, R. Tanzilli, R. Pohl, and J. Vandersande, "The intrinsic thermal conductivity of AIN," *J. Phys. Chem. Solids*, vol. 48, no. 7, pp. 641–647, Jan. 1987, doi: 10.1016/0022-3697(87)90153-3.

[21] P. H. Carey, S. J. Pearton, F. Ren, A. G. Baca, B. A. Klein, A. A. Allerman, A. M. Armstrong, E. A. Douglas, R. J. Kaplar, and P. G. Kotula, "Extreme temperature operation of ultra-wide bandgap AlGaN high electron mobility transistors," *IEEE Trans. Semicond. Manuf.*, vol. 32, no. 4, pp. 473–477, Nov. 2019, doi: 10.1109/tsm.2019.2932074.

[22] X. Hu, S. Hwang, K. Hussain, R. Floyd, S. Mollah, F. Asif, G. Simin, and A. Khan, "Doped Barrier $Al_{0.65}Ga_{0.35}N/Al_{0.40}Ga_{0.60}N$ MOSHFET with SiO_2 gate-insulator and Zr-based ohmic contacts," *IEEE Electron Device Lett.*, vol. 39, no. 10, pp. 1568–1571, Oct. 2018, doi: 10.1109/led.2018.2866027.

[23] J. S. Lundh, B. Chatterjee, J. Dallas, H. Kim, and S. Choi, "Integrated temperature mapping of lateral gallium nitride electronics," in *Proc. 16th IEEE Intersoc. Conf. Therm. Thermomech. Phenomena Electron. Syst. (ITherm)*, May 2017, pp. 320–327, doi: 10.1109/itherm.2017.7992488.

[24] T. Nanjo, A. Imai, Y. Suzuki, Y. Abe, T. Oishi, M. Suita, E. Yagyu, and Y. Tokuda, "AlGaN channel HEMT with extremely high breakdown voltage," *IEEE Trans. Electron Devices*, vol. 60, no. 3, pp. 1046–1053, Mar. 2013, doi: 10.1109/ted.2012.2233742.

[25] J. S. Lundh, B. Chatterjee, Y. Song, A. G. Baca, R. J. Kaplar, T. E. Beechem, A. A. Allerman, A. M. Armstrong, B. A. Klein, A. Bansal, D. Talreja, A. Pogrebnyakov, E. Heller, V. Gopalan, J. M. Redwing, B. M. Foley, and S. Choi, "Multidimensional thermal analysis of an ultrawide bandgap AlGaN channel high electron mobility transistor," *Appl. Phys. Lett.*, vol. 115, no. 15, Oct. 2019, Art. no. 153503, doi: 10.1063/1.5115013.

[26] S. Choi, E. R. Heller, D. Dorsey, R. Vetury, and S. Graham, "The impact of bias conditions on self-heating in AlGaN/GaN HEMTs," *IEEE Trans. Electron Devices*, vol. 60, no. 1, pp. 159–162, Jan. 2013, doi: 10.1109/ted.2012.2224115.

[27] P. Czyz, "Performance evaluation of a 650V E-HEMT GaN power switch," in *Proc. 41st Annu. Conf. IEEE Ind. Electron. Soc. (IECON)*, Nov. 2015, pp. 7–12, doi: 10.1109/iecon.2015.7392939.

[28] I. Omura, W. Saito, T. Domon, and K. Tsuda, "Gallium Nitride power HEMT for high switching frequency power electronics," in *Proc. Int. Workshop Phys. Semiconductor Devices*, Dec. 2007, pp. 781–786, doi: 10.1109/iwpsd.2007.4472634.

[29] S. Choi, G. M. Peake, G. A. Keeler, K. M. Geib, R. D. Briggs, T. E. Beechem, R. A. Shaffer, J. Clevenger, G. A. Patrizi, J. F. Klem, A. Tauke-Pedretti, and C. D. Nordquist, "Thermal design and characterization of heterogeneously integrated InGaP/GaAs HBTs," *IEEE Trans. Compon., Packag., Manuf. Technol.*, vol. 6, no. 5, pp. 740–748, May 2016, doi: 10.1109/tcpmt.2016.2541615.

[30] A. Bar-Cohen, J. J. Maurer, and A. Sivananthan, "Near-junction microfluidic cooling for wide bandgap devices," *MRS Adv.*, vol. 1, no. 2, pp. 181–195, 2016, doi: 10.1557/adv.2016.120.